https://doi.org/10.1016/j.jcsr.2018.09.009

Experimental and numerical investigation on cold-formed steel semi-oval hollow section compression members

Man-Tai Chen [a], Ben Young [b,*]

[a, b] *Department of Civil Engineering, The University of Hong Kong, Pokfulam Road, Hong Kong, China.*

Abstract

A comprehensive experimental and numerical investigation on cold-formed steel semi-oval hollow section pin-ended columns was performed and is presented herein. The semi-oval hollow sections investigated in this study are composed of one semi-circular flange, one flat flange and two flat web plates. Four cross-section sizes were included and a total of 19 tests was conducted under concentric loading with different specimen lengths in the test program. A finite element model was developed and validated against the test results. The numerical model is capable to replicate the test results. Upon the validation of finite element model, an extensive parametric study was performed consisting of 200 numerical data cases, which cover a wide range of cross-section geometries and column slenderness. The results obtained from experimental program and numerical study were compared with the predicted strengths by the existing and modified Direct Strength Method. Reliability analysis was conducted to assess the reliability of the design methods. The comparison results show that the existing Direct Strength Method generally provides conservative predictions, but the predictions are scattered for slender sections. Modification was proposed to address this issue. The modified Direct Strength Method provides accurate and less scattered predictions in a reliable manner. The modified Direct Strength Method is suitable for cold-formed steel semi-oval hollow section columns, especially for short column members and columns with slender sections.

Keywords: Cold-formed; Direct Strength Method; Finite element; Pin-ended columns; Semi-oval hollow sections; Structural design.

---

* Corresponding author. Tel.: +852-2859-2674; fax: +852-2559-5337.
E-mail address: young@hku.hk (B. Young).

1. Introduction

The semi-oval hollow section (SOHS) investigated in this study is a novel tubular section type, which is composed of one semi-circular flange, one flat flange and two flat web plates. Unlike the circular and square hollow sections, the possession of different geometric properties about the two principal axes allows the SOHS to be oriented to achieve better loading resistance. Compared with the rectangular hollow section, the SOHS has a semi-circular portion, which offers the aesthetic appearance and is able to provide larger local buckling resistance than the flat plate [1, 2]. The complementary qualities of aesthetically pleasing appearance and the superior structural efficiency of SOHS offer an interesting alternative to engineers and architects especially for exposed steelwork. The SOHS has been adopted to decorate the façade supporting members as shown in Fig. 1, which manifests its attractiveness in architectural perspective. Nevertheless, even though the SOHS has prominent advantages in both structural and aesthetical aspects, there is scarce investigation and a lack of design information available for this newly developed section type.

Previously, Chen and Young [3] have conducted experimental and numerical investigation on the cross-sectional behavior of cold-formed steel semi-oval hollow section stub columns compressed between fixed ends and proposed design rules for SOHS stub columns. However, the structural behavior of cold-formed steel SOHS pin-ended column members remains unexplored.

The aim of this paper is to investigate the structural behavior of cold-formed steel semi-oval hollow section pin-ended column members in both experimental and numerical manners. In the test program, a total of 19 column tests was conducted between pinned ends. The specimen length of test specimens was designed to vary from 200 mm to 1500 mm in order to cover a range of column length. In addition, a non-linear finite element (FE) model was developed and validated against the test results. An extensive parametric study comprising 200 column specimens was performed based on the validated FE model to expand the range of cross-section geometries and column slenderness of

cold-formed steel SOHS column members.

The current design specifications for steel structures [4-7] do not cover the cross-section classification and the effective width calculation for cold-formed steel SOHS investigated in this study. Unlike traditional design methods, the Direct Strength Method (DSM) as detailed in the AISI S100-16 [5] can be used to calculate the design strength of column member with arbitrary cross-section profile. However, the DSM design equations were originally calibrated by open sections with plate elements, the applicability and reliability of the DSM for the column strength predictions of the cold-formed steel SOHS members are questionable and were evaluated in this study. The results obtained from experimental and numerical investigation were used to compare with the design strength predictions by the Direct Strength Method and to propose modification on Direct Strength Method for cold-formed steel SOHS columns. The applicability and reliability of the existing and modified DSM were examined through reliability analysis.

2. Experimental investigation

2.1. Test specimens

The test specimens consisted of 19 pin-ended columns. All the SOHS investigated in this study were cold-formed from hot-extruded seamless steel circular hollow sections. The test specimens are categorized into four series according to the cross-section geometry of SOHS as defined using the nomenclature in Fig. 2. The nominal dimensions ($D\times B\times t$) of SOHS are 93×62×5.5, 107×68×6.5, 108×79×5.5 and 125×85×6.5, where D, B, t are the overall depth, overall width and wall thickness of the sections, respectively. The nominal cross-section aspect ratio (D/B) of the specimens varies slightly from 1.37 to 1.57. All the SOHS are labeled such that the nominal cross-section geometry, the specimen type and the specimen length can be identified. The letters C in the last part of the specimen label indicates a pin-ended column. The following letter L together with the number designates the length of the actual specimen, whereas the symbol # denotes a repeated test. The measured specimen dimensions are reported in Table 1, where r_o and r_i are the external and internal

corner radii, respectively, and L is the actual specimen length.

2.2. Material properties

Material properties of cold-formed steel semi-oval hollow sections were determined by tensile coupon tests at three critical locations, i.e. flat web, tip of semi-circular portion and the corner. The obtained material properties were incorporated into the numerical study and were used in the design strength predictions. The results of the tensile coupon tests are reported by Chen and Young [3], while a summary of the test results is presented in Table 2.

2.3. Geometric imperfection measurements

The initial global geometric imperfections ω_g of the pin-ended columns were obtained based on the measurements taken on flat flange near the corner at mid-height and near both ends of the specimens in the buckling direction using a Leica TCR405 total-station prior to testing. The initial global imperfection is positive when the specimen is bowed in the same direction as the bending direction, and vice versa. The measured values are reported in Table 1. The average absolute value of the normalized initial global imperfection at mid-length was 1/12606 for the test column specimens. The negligibly small value of initial global geometric imperfection demonstrates the great straightness of the tubes.

2.4. Test setup and procedure

A total of 19 column tests was conducted as pin-ended to examine the load-carrying capacity and load-end shortening history of the cold-formed steel SOHS. The column samples were cut to specified specimen lengths of 200, 440, 850, 1200 and 1500 mm with both ends milled flat before welding of 25.4 mm thick end plates.

The test setup and test rig of pin-ended columns of various lengths are shown in Figs. 3 and 4. A special bearing system, which consists of a pair of pit plates with V-shaped grooves and wedge

plates with knife-edges, was designed to replicate pinned end conditions and to allow free rotations about major axis as well as to restrain rotations about the orthogonal axis. The specimens were adjusted on the slotted wedge plates to a designated eccentricity (the aimed eccentricity of zero for column tests in this case) before being bolted to the wedge plates. For the test setup of columns with actual specimen lengths of 850, 1200 and 1500 mm, the upper pit plate was fixed and the lower one was installed on a special ball bearing at the bottom as shown in Fig. 4. Before testing, a small preloading of 3 to 5 kN was applied to eliminate any possible gaps between the wedge plates and the pit plates as well as to ensure everything was in full contact and the specimen was in an up-right position. The special ball bearing was then locked by horizontal and vertical bolts to restrain the bearing from twisting and rotation, respectively. Considering the higher loading resistances for the short column specimens with actual specimen lengths of 200 and 440 mm, another hydraulic testing machine was used. The test setup is similar to that for the other column tests but a different lockable sitting was adopted as shown in Fig. 3.

Three LVDTs were installed to measure both the end shortening and end rotation of the specimens. In addition, two LVDTs were installed at the mid-height of the specimen on the two sides in the bending plane to capture the real-time horizontal deflection of the columns during loading. To determine the loading eccentricities, three strain gauges were attached on two faces in the bending plane at the mid-height of each specimen, to be more specific, one at the tip of semi-circular flange and two on the flat flange near the corners, at which the extreme compressive and tensile fibers located, as shown in Fig. 5. The applied load, readings of strain gauges and lateral deflection in the bending direction at mid-height were recorded to derive the actual loading eccentricity of the specimen. During the initial stage of the test, the bending moments of the specimens at mid-height can be expressed as $P(e+\omega_g+\Delta)$ or $EI_y\kappa$ within the elastic range. By equating $EI_y\kappa$ with $P(e+\omega_g+\Delta)$, the measured loading eccentricity including the initial global geometric imperfection can be determined by $(e+\omega_g)=EI_y\kappa/P-\Delta$, where EI_y is the flexural rigidity of the cross-section about the major axis, κ is the curvature of the specimen and is expressed as the strain gradient of the section

under bending, P is the applied compressive load, e is the eccentricity at specimen ends, ω_g is the initial global geometric imperfection and Δ is the lateral deflection of specimen at mid-height in the bending direction. With reference to the readings of strain gauges under a certain amount of preloading within elastic range, the position of specimen was further adjusted until an acceptable eccentricity was achieved. Although the eccentricities of column specimens were aimed at zero, there existed an unintentional eccentricity for each specimen, the values of which are reported in Table 3. The largest measured eccentricity ($e+\omega_g$) of 0.56 mm and the average measured eccentricity of 0.21 mm indicate the excellent alignment of the column specimens. Displacement controlled loading with a constant speed of 0.5 mm/min was used to apply the axial compression load to the specimens. The applied displacement was paused for 100 seconds near the ultimate load to obtain the static responses of specimens. The load, readings from LVDTs and strain gauges were recorded at one second intervals by a data acquisition system.

2.5. Test results

The experimental load-carrying capacities, the effective lengths and the measured eccentricities of column specimens are reported in Table 3. The effective length (L_e) of the pin-ended column specimen was measured between the tips of knife-edged wedges at two ends as shown in Figs. 3 and 4, which is equal to the sum of specimen length, the thicknesses of two end plates (50.8 mm) and the heights of the two wedge plates (122.8 mm). It is found that the results of repeated tests are very close to their corresponding first test values by the differences of 1.9% and 2.3% for column specimens 108×79×5.5-CL440 and 108×79×5.5-CL1500, respectively. Therefore, the reliability of the test results was demonstrated by the small differences between the repeated test values and their corresponding first test values.

The failure modes observed in the pin-ended column tests involved cross-section yielding (Y) and flexural buckling (F) as shown in Table 3. To distinguish whether the column was failed by cross-section yielding, the squash load (P_y^) of the column specimen, which is calculated as the sum of the

0.2% proof stresses at the flat, semi-circular and corner portions multiplied by their corresponding cross-section areas, is compared with its ultimate load-carrying capacity. The failure mode of column was considered to be cross-section yielding when the ultimate strength is greater than the squash load of the column specimen. It is shown in Table 3 that the ratio of ultimate strength to squash load for all SOHS short column specimens with actual specimen lengths of 200 and 440 mm is greater than unity, which indicates that all the SOHS short columns failed by cross-section yielding, hence the SOHS investigated herein are considered as compact sections. With the greater column lengths, flexural buckling failures appeared as expected and the ultimate load-carrying capacity of pin-ended columns will decrease with the increase in column length. The static load-end shortening responses for typical SOHS pin-ended column specimens are depicted in Fig. 6.

3. Finite element model

Finite element model using the program ABAQUS of version 6.14 was developed to simulate the pin-ended column tests conducted on cold-formed steel SOHS. In the validation of FE model, the measured cross-section geometries and material properties were used. Full length of actual specimen was modeled.

To simulate the pin-ended boundary condition of the test column specimens, the displacements of cross-section edges at both ends of column specimen were coupled to the displacements of the corresponding reference points located at 86.8 mm away from the specimen edges. The value of 86.8 mm corresponds to the sum of the end-plate thickness and the height of one wedge plate. The measured loading eccentricity was also included in the finite element model by offsetting the reference point from the center of the cross-section. The reference points were restrained against all other degrees of freedom, excluding the longitudinal displacement at the loading point and the major axis rotation at two ends. The compressive load was applied by specifying the axial displacement of the reference point corresponding to the loading end using a static RIKS step. The nonlinear

geometric parameter (*NLGEOM) was enabled to allow for large displacement analysis.

A four-node shell element with reduced integration (S4R) was selected to model the SOHS pin-ended columns. The value of (B+D)/30 was taken as the mesh size in the flat and semi-circular portions, whilst finer mesh was used for corner regions. The mesh was assigned uniformly along longitudinal direction of the specimen.

The residual stresses induced from the cold-forming process consist of bending residual stress and membrane residual stress. Since the bending residual stress, which has the larger magnitude and more significant effect than membrane residual stress, has already been included into the measured material properties from coupon tests, it is rational not to incorporate the residual stresses explicitly into the finite element model [3, 8-11].

Significant strength enhancement was introduced to the corner region due to the cold working effect. The strength enhancement is not limited to the corner region, but extended to a certain distance away from the corner. Therefore, the sensitivity analysis was performed to determine the extension of corner strength enhancement region. The corner was extended by t, 2t and 2.5t in the sensitivity analysis. Table 4 summarizes the comparison results of the sensitivity analysis and shows that different corner extensions provide very similar prediction with less than 1% difference on average. The corner strength enhancement was extended into the adjacent flat portions by a distance of 2t in the model, which is consistent with the value taken in SOHS stub column model [3].

The local and global geometric imperfections were included in the FE model. The lowest elastic local and global buckling mode shapes obtained by eigenvalue analysis were taken as the initial local and global geometric imperfection profiles of the column, and the local and global buckling mode shapes were amplified by the corresponding magnitudes and were further superimposed on the column model. The sensitivity study was also performed for pin-ended column members as shown

in Table 4 to determine the suitable magnitudes of the imperfections to be adopted in the further parametric study. Two magnitudes of local imperfection (t/16 and t/50) and two magnitudes of global imperfection (L/1500 and L/3500) were considered herein. The models with different magnitudes of local and global imperfections provide similar predictions with less than 1% difference on average. The magnitude of t/50 was selected for local imperfection in the parametric study, which is consistent with the value taken in SOHS stub column model [3]. The magnitude of L/3500 was selected for global imperfection of column specimens in the model.

4. Validation of finite element model

The finite element model of pin-ended columns was developed and verified against 19 column tests. The results of validation for the final adopted model using 2t corner extension and imperfection combination of t/50+L/3500 (local+global) are shown in the last column of Table 4. The mean value and coefficient of variation (COV) of the test-to-FE strength ratio are 1.03 and 0.051, respectively. This demonstrates that the FE model can accurately predict the axial loading capacities of cold-formed steel SOHS pin-ended columns. The experimental and numerical load-end shortening responses as well as the failure modes for typical test specimens were compared as depicted in Figs. 7-9.

5. Parametric study

Material properties obtained from the three critical locations of SOHS 107×68×6.5 were used in the FE analysis. Together with the aforementioned modeling parameters and assumptions, parametric study on 200 cold-formed steel SOHS pin-ended column specimens was performed using the validated FE model. Extensive range of cross-section geometries and column slenderness was designed for the parametric study, including 40 different cross-sections with 5 different column lengths for each section. The cross-section aspect ratio (D/B) of the SOHS varies from 1.25 to 2.50

and the thickness of the section was designed to cover a wide range of cross-section slenderness ratio from stocky to slender sections. The lengths of the column specimens were designed to cover a spectrum of column slenderness ($\lambda=L_e/r$) ranging from 8.3 to 89.6. The load carrying capacities of cold-formed steel SOHS pin-ended columns obtained from the numerical study are summarized in Table 5. The numerical results together with the test results were used for the assessment of existing and modified DSM for cold-formed steel SOHS pin-ended columns.

6. Reliability analysis

The reliability of the existing and modified design methods was evaluated through reliability analysis. The details of reliability analysis are specified in the North American Specification AISI S100-16 [5]. The design method is considered to be reliable if the resulted reliability index (β) is not less than 2.5. In the calculation of reliability index, the values of statistical parameters (M_m=1.1, F_m=1.0, V_M=0.1, V_F=0.05 and V_Q=0.21) are specified in the AISI S100-16 [5]. The calibration coefficient in the reliability index calculation depends on the load combination specified in the design specification. The axial loading capacities of column members obtained from test program and numerical study were compared with the design strength prediction by the Direct Strength Method as detailed in the AISI S100-16 [5]. The load combination of 1.2DL+1.6LL was used in the reliability analysis for the Direct Strength Method, where DL means the dead load and LL means the live load. The value of resistance factor ϕ is 0.85 for the Direct Strength Method. The calculated reliability indices of existing and modified DSM for compressive strength predictions of cold-formed steel SOHS pin-ended columns are shown in Table 6.

7. Assessment of the current Direct Strength Method

7.1 General

The existing traditional design methods for steel structures [4-7] do not cover the cross-section classification and effective width calculation of cold-formed steel SOHS and hence, do not cover the

structural design for such section. The finite strip method suggested by the Direct Strength Method [5] is applicable to arbitrary cross-sections for critical elastic buckling stress predictions. However, since the DSM design equations were originally calibrated by open sections with plate elements, the applicability and reliability of the DSM for the design strength predictions of the cold-formed steel SOHS pin-ended columns are questionable and were therefore evaluated in this study. The experimental and numerical results were used to compare with the nominal strengths (unfactored design strengths) predicted by the Direct Strength Method [5]. The material properties obtained from tensile coupon tests in the location with lowest 0.2% proof stress were used in nominal strength calculation for conservative prediction.

Before evaluating the nominal axial strengths of pin-ended columns, the effect of the additional bending moments induced by the unintentional eccentricities on the design strengths was quantified by comparing the column design strengths calculated by considering the ideal case with zero eccentricity with the counterpart calculated by considering measured eccentricities ($e+\omega_g$). However, the design specifications for member under combined compression and bending are not included in the DSM. In this case, the interaction equation for member under combined compression and bending as detailed in Clause H1.2 of the AISI S100-16 [5] was adopted for design strength calculation with the nominal axial strength and nominal flexural strength determined from the DSM. Based on this method, the average differences between the two calculations for sections 93×62×5.5, 107×68×6.5, 108×79×5.5 and 125×85×6.5 are 1.5%, 1.1%, 1.1% and 1.1%, respectively. The small difference for each section indicates that the columns were properly aligned and the effect of unintentional eccentricity on column strength prediction is small.

7.2 Direct Strength Method

The Direct Strength Method for column design is detailed in Chapter E of the AISI S100-16 [5]. The nominal axial strength is determined by the minimum of the nominal axial strengths for

flexural, torsional or flexural-torsional buckling as well as local buckling and distortional buckling. No distortional buckling was observed from the tests. The critical elastic local buckling load was obtained from CUFSM program using the finite strip method [12] with a 1 mm half-wave length interval and that for overall buckling was obtained in accordance with AISI S100-16 [5]. Short and long SOHS columns with both slender and non-slender cross-sections were included in this study. The mean value of P_u/P_{DSM} is 1.01 with the corresponding COV of 0.104 as shown in Table 6. The reliability index is 2.64, which is larger than 2.5. It is found that the existing Direct Strength Method provides generally conservative and reliable predictions for cold-formed steel SOHS columns. Nevertheless, the nominal strength predictions by existing DSM are quite conservative for short SOHS columns (column slenderness of $\lambda_c \leq 0.25$) with non-slender sections having the mean value of P_u/P_{DSM} equal to 1.17, and the predictions are quite scattered for SOHS columns with slender sections (cross-section slenderness of $\lambda_l > 0.702$) with the COV of 0.104 as shown in Table 6 and Fig. 10. To cater for these issues, modification on the existing DSM can be developed as presented in the next section.

8. Modified Direct Strength Method

Although the existing DSM is capable to provide generally conservative and reliable nominal strength predictions for cold-formed steel SOHS columns, there still exists room for improvement. Modification on the DSM is proposed in this study to cater for the scatteredness of strength predictions for columns with slender sections and the conservativeness of short column strength predictions.

The slenderness factors for local (λ_l) and flexural buckling (λ_c) of column are defined in Eqs. (1) and (2), respectively.

$$\lambda_l = \sqrt{\frac{P_y}{P_{crl}}} \tag{1}$$

$$\lambda_c = \sqrt{\frac{f_y}{f_{cre}}} \tag{2}$$

where P_y is the squash load ($P_y = f_y A$), P_{crl} is the critical elastic local buckling load of column, f_y is the yield stress and f_{cre} is the critical elastic buckling stress for flexural buckling as determined by Eq. (3).

$$f_{cre} = \frac{\pi^2 E}{(L_e/r)^2} \tag{3}$$

where r is the radius of gyration of the full cross-section. The design strength predicted by the modified Direct Strength Method (P_{DSM}*) is taken as the minimum of P_{nl}* and P_{ne}* calculated as per Eqs. (4)-(9), which consider the effects of local and flexural buckling, respectively. The effect of shift of effective centroid for the slender section has been included in the design equations as shown in Eqs. (6)-(9) through two factors, namely K and R, the values of which are correlated to the cross-section slenderness factor (λ_l).

$$P_{nl}{}^* = \begin{cases} 1.2P_y & \text{for } \lambda_l \le 0.472 \\ \left[1 - 0.168\left(\frac{P_{crl}}{P_y}\right)^{0.34}\right]\left(\frac{P_{crl}}{P_y}\right)^{0.34} P_y & \text{for } \lambda_l > 0.472 \end{cases} \tag{4}$$

For non-slender section with $\lambda_l \le 0.702$:

$$P_{ne}{}^* = \begin{cases} (1.2 - 0.6\lambda_c)P_y & \text{for } \lambda_c \le 0.5 \\ \left(\frac{0.877}{\lambda_c{}^2}\right) P_y & \text{for } \lambda_c > 0.5 \end{cases} \tag{5}$$

For slender section with $\lambda_l > 0.702$:

$$P_{ne}{}^* = \begin{cases} \left(KQ^{\lambda_c{}^R}\right) P_{nl}{}^* & \text{for } \lambda_c \le 2 \\ \left(\frac{0.877}{\lambda_c{}^2}\right) P_y & \text{for } \lambda_c > 2 \end{cases} \tag{6}$$

$$K = 1.05 - 0.1\lambda_l \tag{7}$$

$$R = 2.5 - 0.25\lambda_l \tag{8}$$

$$Q = \left(\frac{0.21925}{K}\right)^{\frac{1}{2^R}} \quad (9)$$

To assess the applicability of the modified Direct Strength Method for design strength predictions of cold-formed steel SOHS columns, the mean value and COV of P_u/P_{DSM}* were evaluated and the reliability analysis was conducted. The comparison results are shown in Table 6 and Fig. 11. The mean value of P_u/P_{DSM}* is 1.03 with the corresponding COV of 0.069. It can be found from Table 6 and Fig. 11 that the modified DSM is able to provide conservative and less scattered design strength predictions especially for columns with slender sections, and improve the accuracy of design strength predictions for short columns. With the resistance factor of 0.85, the reliability index is 2.85, which is larger than the targeted value of 2.5 indicating that the modified DSM is reliable in the column strength predictions of cold-formed steel SOHS.

9. Conclusions

The structural behavior of cold-formed steel semi-oval hollow section pin-ended columns was investigated experimentally and numerically. A series of tests were conducted on SOHS columns with different specimen lengths compressed between pinned ends. Upon the validation of finite element model against the test results, a comprehensive parametric study, which covers a wide range of cross-section geometries and column slenderness, was performed to study the behavior of cold-formed steel semi-oval hollow section pin-ended columns. The results obtained from experimental program and numerical study were compared with the predicted strengths by the existing and modified Direct Strength Method. The comparison results show that the existing Direct Strength Method provides conservative predictions for cold-formed steel semi-oval hollow section columns in general, but the predictions are scattered for columns with slender sections and quite conservative for short columns. To address these issues, modification is proposed in this study. The modified method generally improves the design strength predictions especially for short column members, and

is able to provide accurate and less scattered design strength predictions in a reliable manner. The modified Direct Strength Method is suitable for cold-formed steel semi-oval hollow section columns, especially for short column members and columns with slender sections.

Acknowledgements

The authors are grateful to Shenyang Dongyang Special Section Tube for supplying the test specimens. The research work described in this paper was supported by a grant from the Research Grants Council of the Hong Kong Special Administrative Region, China (Project No. 17267416).

Nomenclature

A	Area of full cross-section
B	Overall width of the section
COV	Coefficient of variation
D	Overall depth of the section
DL	Dead load
DSM	Direct strength method
E	Young's modulus
e	Loading eccentricity of pin-ended column specimen
I_y	Moment of inertia about the major axis (see Fig. 2)
FE	Finite element
F_m	Mean value of fabrication factor
f_{cre}	Critical elastic buckling stress for flexural buckling
f_y	Yield stress
L	Actual specimen length
L_e	Effective length of column
LL	Live load
M_m	Mean value of material factor
P	Applied axial compression
P_{crl}	Critical elastic local buckling load of column
P_{DSM}	Nominal axial strength of column predicted by the Direct Strength Method
P_{DSM}*	Nominal axial strength of column predicted by the modified Direct Strength Method
P_{Exp}	Experimental loading capacity
P_{FE}	Finite element loading capacity
P_{ne}*	Modified nominal axial strength of column for flexural buckling
P_{nl}*	Modified nominal axial strength of column for local buckling
P_u	Ultimate axial loading capacity

P_y	Squash load of cross-section
P_y^	Squash load of cross-section considering the cold-forming enhancement
r	Radius of gyration
r_i	Inner corner radius of the section
r_o	Outer corner radius of the section
SOHS	Semi-oval hollow section
t	Thickness of the section
V_F	Coefficient of variation of fabrication factor
V_M	Coefficient of variation of material factor
V_Q	Coefficient of variation of load effect
β	Reliability index
Δ	Lateral deflection of specimen at mid-height in the bending direction
ε_f	Tensile strain at fracture
ϕ	Resistance factor
κ	Curvature of the specimen
λ	Column slenderness
λ_c	Slenderness factor for flexural buckling
λ_l	Slenderness factor for local buckling
σ_u	Static ultimate tensile strength of material
$\sigma_{0.2}$	Static 0.2% tensile proof stress of material
ω_g	Initial global geometric imperfection

References

[1] Zhu JH, Young B. Cold-formed-steel oval hollow sections under axial compression. Journal of Structural Engineering 2011;137(7):719-727.

[2] Zhu JH, Young B. Design of cold-formed steel oval hollow section columns. Journal of Constructional Steel Research 2012;71:26-37.

[3] Chen MT, Young B. Cross-sectional behavior of cold-formed steel semi-oval hollow sections. Engineering Structures 2018;(In press).

[4] ANSI/AISC-360 2016. Specification for Structural Steel Buildings. *ANSI/AISC 360-16.* Chicago, IL, USA: American Institute of Steel Construction.

[5] AISI-S100 2016. North American Specification for the design of cold-formed steel structural members. *AISI S100-16.* Washington,D.C., USA: American Iron and Steel Institute.

[6] AS/NZS-4600 2005. Cold-formed steel structure. *AS/NZS 4600:2005.* Sydney, Australia: Standards Australia/Standards New Zealand.

[7] EN1993-1-1 2005. Design of steel structures–Part 1.1: General rules and rules for buildings. *EN 1993-1-1:2005.* Brussels, Belgium: European Committee for Standardization.

[8] Huang Y, Young B. Experimental and numerical investigation of cold-formed lean duplex stainless steel flexural members. Thin-Walled Structures 2013;73:216-228.

[9] Huang Y, Young B. Structural performance of cold-formed lean duplex stainless steel columns. Thin-Walled Structures 2014;83:59-69.

[10] Ma JL, Chan TM, Young B. Experimental Investigation on Stub-Column Behavior of Cold-Formed High-Strength Steel Tubular Sections. Journal of Structural Engineering 2015;142(5):04015174.

[11] Zhao O, Rossi B, Gardner L, Young B. Behaviour of structural stainless steel cross-sections under combined loading–Part II: Numerical modelling and design approach. Engineering Structures 2015;89:247-259.

[12] Schafer BW, Ádány S. Buckling analysis of cold-formed steel members using CUFSM: conventional and constrained finite strip methods. In: Eighteenth international specialty

conference on cold-formed steel structures, Orlando, FL, USA; 2006. p. 39-54.

(a) Overall view of facade decoration

(b) Detail of facade decoration

Fig. 1. Decoration of facade supporting system of Garden City in Shenzhen, China

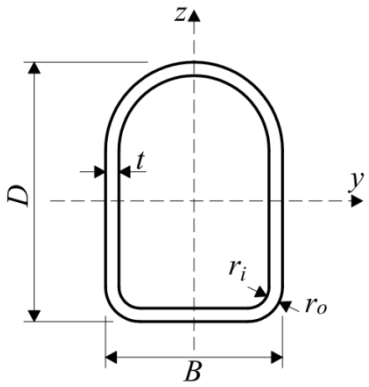

Fig. 2. Cross-section geometry of SOHS

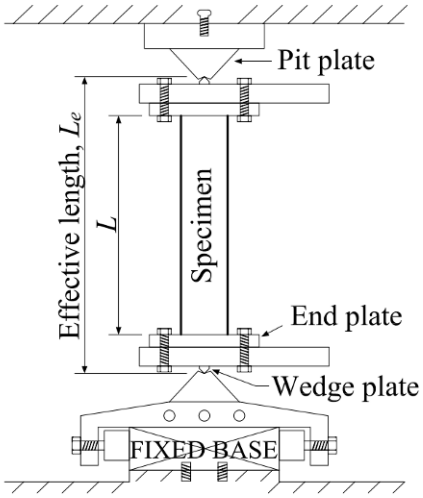

(a) Schematic view (b) Experimental arrangement

Fig. 3. Test setup and test rig for pin-ended columns with actual specimen lengths of 200 and 440 mm

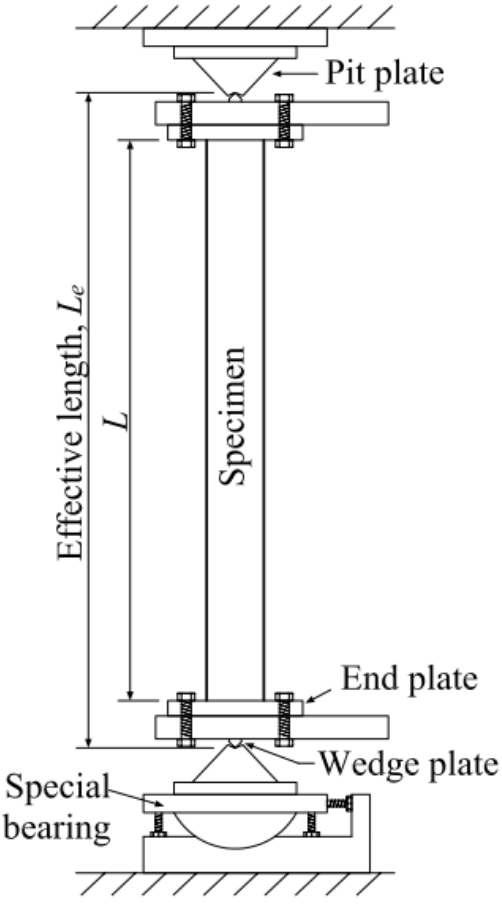

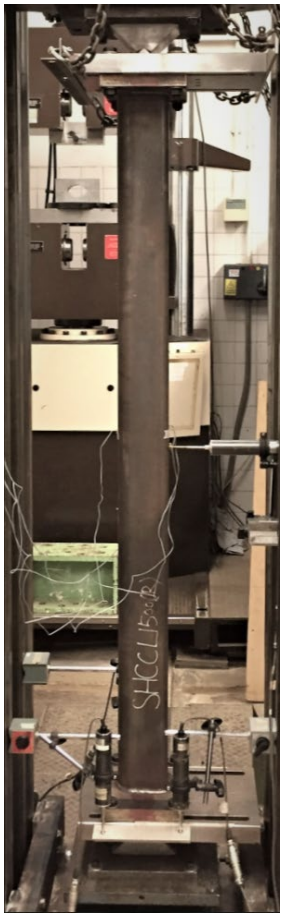

(a) Schematic view (b) Experimental arrangement

Fig. 4. Test setup and test rig for pin-ended columns with actual specimen lengths of 850, 1200 and 1500 mm

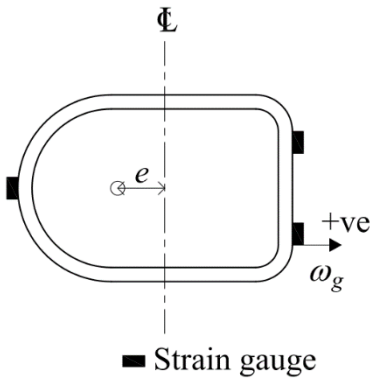

Fig. 5. Strain gauge arrangement

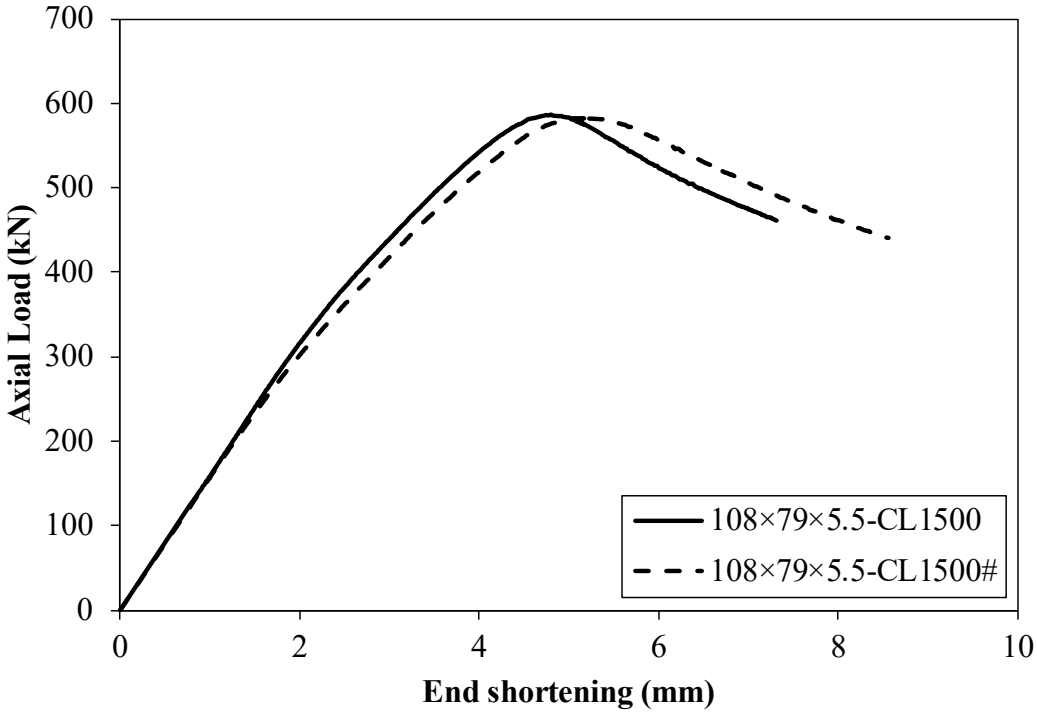

Fig. 6. Load-end shortening responses for typical SOHS pin-ended column specimens 108×79×5.5-CL1500 and 108×79×5.5-CL1500#

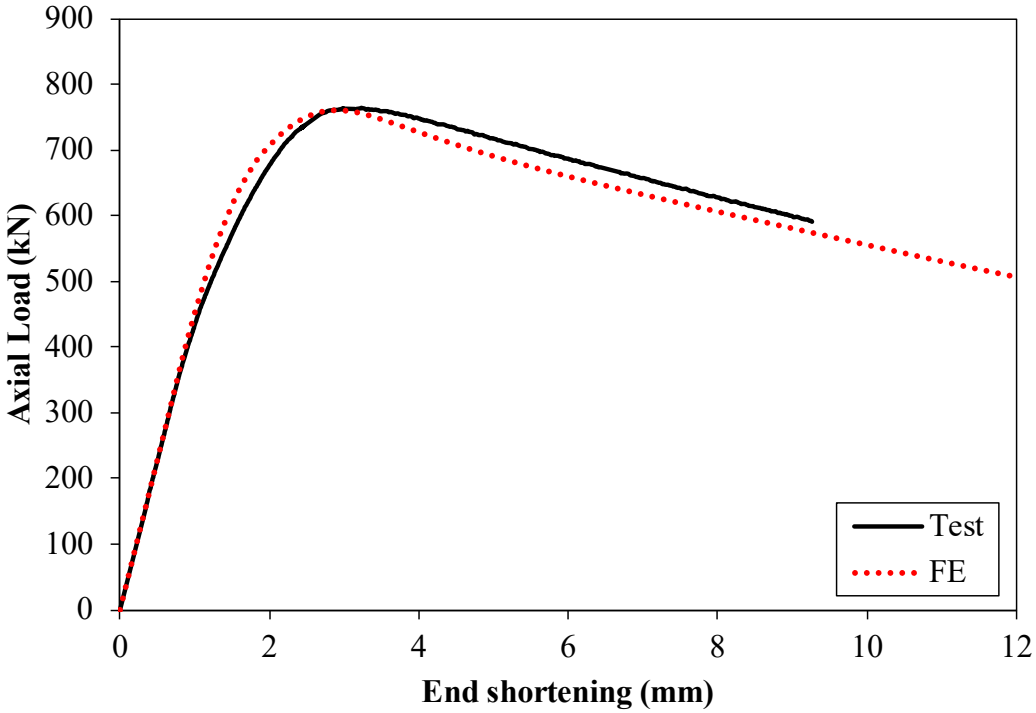

Fig. 7. Comparison between test and finite element results of load-end shortening response for typical SOHS pin-ended column specimen 107×68×6.5-CL850

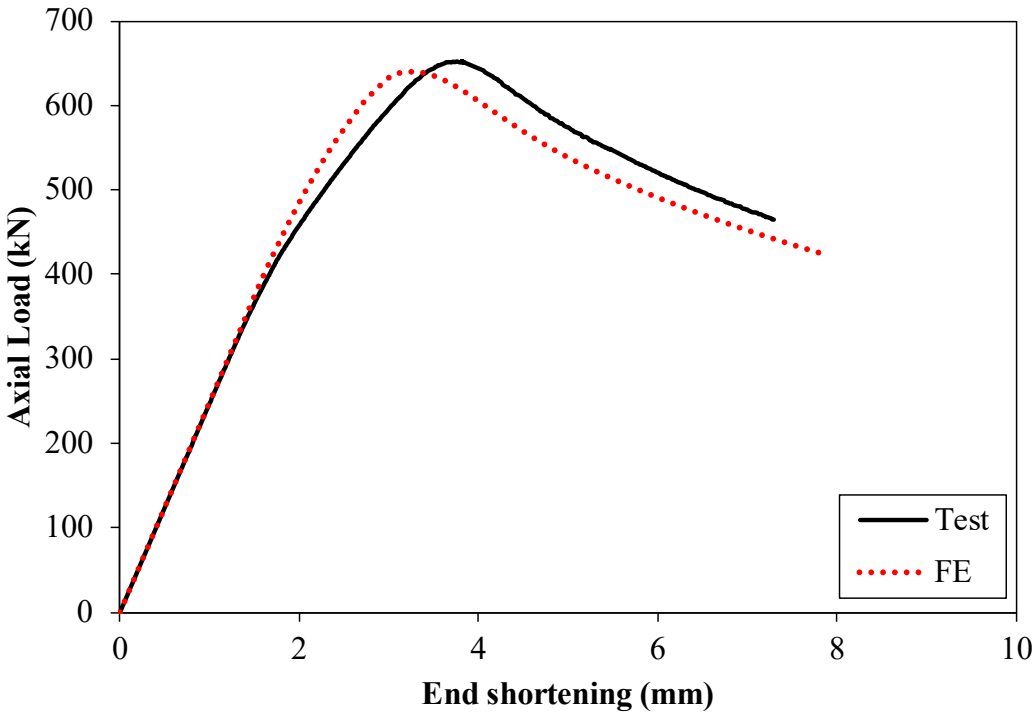

Fig. 8. Comparison between test and finite element results of load-end shortening response for typical SOHS pin-ended column specimen 107×68×6.5-CL1500

Fig. 9. Comparison between experimental and numerical failure modes for column specimen 107×68×6.5-CL1500

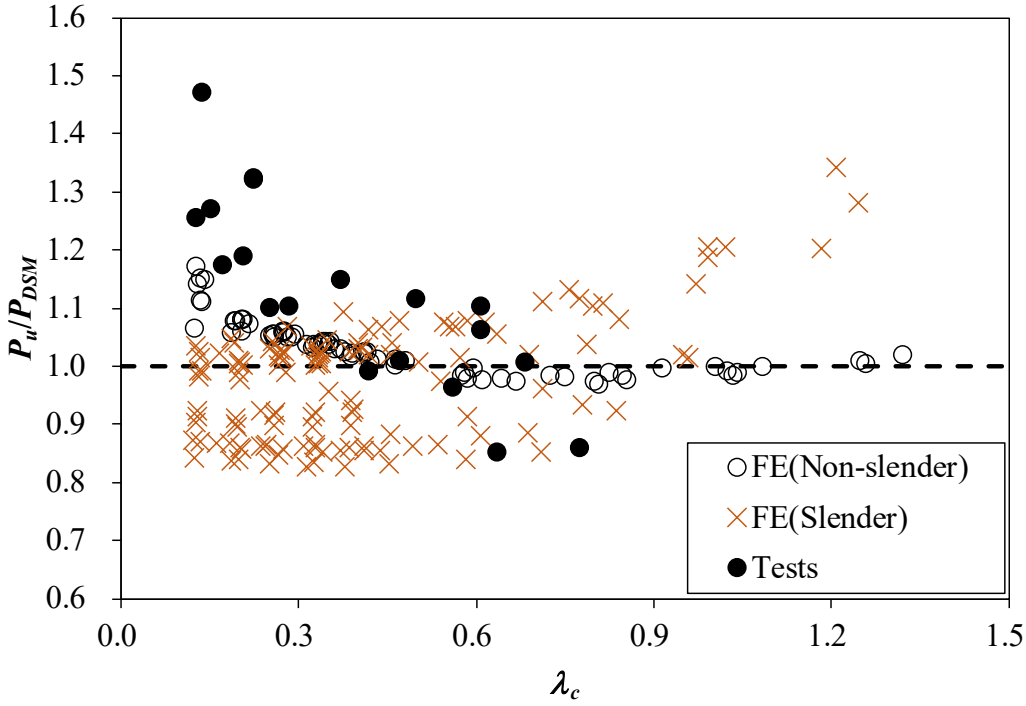

Fig. 10. Comparison of test and FE results with the DSM predictions

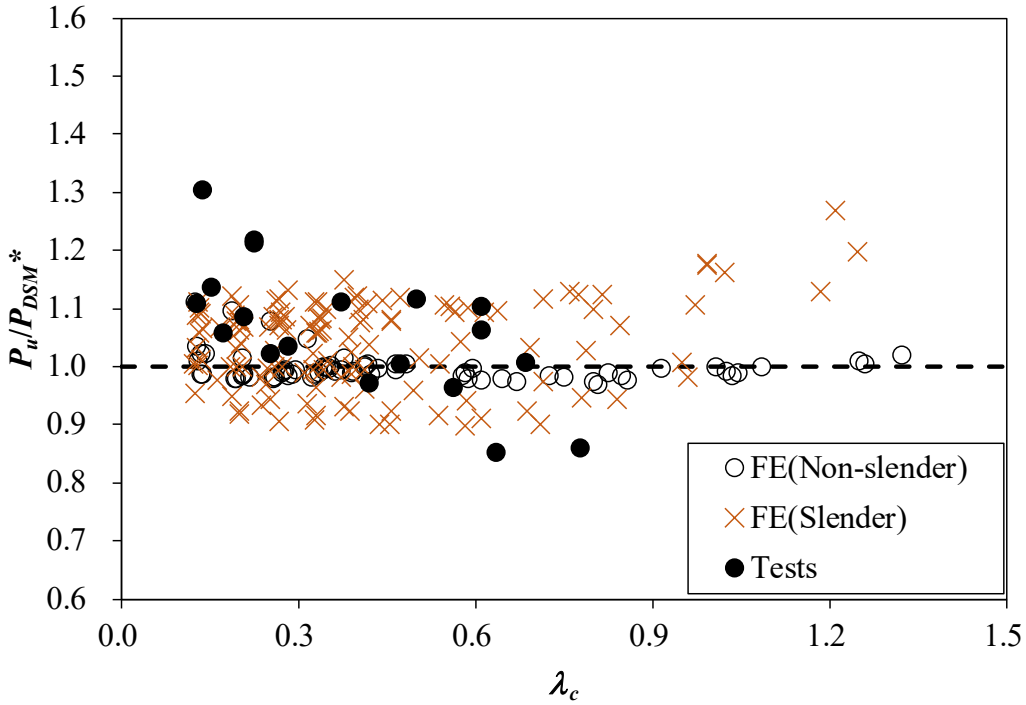

Fig. 11. Comparison of test and FE results with the modified DSM predictions

Specimen	D (mm)	B (mm)	t (mm)	r_o (mm)	r_i (mm)	L (mm)	ω_g (mm)	ω_g/L
93×62×5.5-CL200	93.6	61.9	5.43	14.5	9.0	200	0	0
93×62×5.5-CL440	93.3	62.1	5.12	14.4	9.3	440	0	0
93×62×5.5-CL850	93.3	62.0	5.13	14.5	9.4	850	0	0
93×62×5.5-CL1200	93.3	62.0	5.40	14.4	9.1	1200	0	0
93×62×5.5-CL1500	93.4	61.9	5.58	15.4	9.8	1500	0	0
107×68×6.5-CL200	107.3	68.0	6.15	16.8	10.7	200	0.01	1/34946
107×68×6.5-CL440	107.4	67.9	6.39	16.4	10.0	440	0.26	1/1690
107×68×6.5-CL850	107.5	67.8	6.40	16.0	9.6	850	0.25	1/3346
107×68×6.5-CL1200	107.2	67.9	6.18	15.6	9.4	1200	0	0
107×68×6.5-CL1500	107.3	68.0	6.16	16.1	9.9	1500	0	0
108×79×5.5-CL200	108.3	79.0	5.57	12.7	7.1	200	0	0
108×79×5.5-CL440	108.4	79.0	5.59	13.0	7.4	440	0	0
108×79×5.5-CL440#	108.3	79.1	5.50	13.5	8.0	440	0	0
108×79×5.5-CL850	108.4	78.9	5.55	13.7	8.2	850	0	0
108×79×5.5-CL1200	108.3	79.0	5.46	12.6	7.1	1200	0	0
108×79×5.5-CL1500	108.3	79.0	5.53	13.3	7.7	1500	0	0
108×79×5.5-CL1500#	108.5	79.1	5.62	13.9	8.3	1500	0.25	1/5906
125×85×6.5-CL200	124.9	85.0	6.45	16.9	10.5	200	0	0
125×85×6.5-CL440	124.9	85.1	6.45	16.7	10.2	440	0.08	1/5774

Table 1. Measured dimensions and global imperfections of SOHS pin-ended columns

Section	Flat (TC1)				Curved (TC2)				Corner (TC3)			
	E (GPa)	$\sigma_{0.2}$ (MPa)	σ_u (MPa)	ε_f (%)	E (GPa)	$\sigma_{0.2}$ (MPa)	σ_u (MPa)	ε_f (%)	E (GPa)	$\sigma_{0.2}$ (MPa)	σ_u (MPa)	ε_f (%)
93×62×5.5	204	453	549	22	211	444	551	23	211	511	600	16
107×68×6.5	211	475	548	20	209	450	540	26	210	518	605	16
108×79×5.5	206	460	555	27	199	366	545	26	185	507	625	17
125×85×6.5	207	439	530	26	204	419	531	28	203	486	577	19

Table 2. Measured material properties obtained from tensile coupon tests [3]

Specimen	$e+\omega_g$ (mm)	L_e (mm)	P_{Exp} (kN)	Failure mode	P_y^ (kN)	$\frac{P_{Exp}}{P_y}$^
93×62×5.5-CL200	0.34	374	715.1	Y	635.2	1.13
93×62×5.5-CL440	0.08	614	620.6	Y	599.8	1.03
93×62×5.5-CL850	0.02	1024	536.0	F	600.8	0.89
93×62×5.5-CL1200	0.25	1374	440.4	F	630.8	0.70
93×62×5.5-CL1500	0.56	1674	420.2	F	649.6	0.65
107×68×6.5-CL200	0.20	374	1002.1	Y	836.7	1.20
107×68×6.5-CL440	0.03	614	885.0	Y	868.0	1.02
107×68×6.5-CL850	0.09	1024	764.3	F	870.1	0.88
107×68×6.5-CL1200	0.05	1374	677.1	F	841.4	0.80
107×68×6.5-CL1500	0.43	1674	660.8	F	838.8	0.79
108×79×5.5-CL200	0.08	374	929.0	Y	747.2	1.24
108×79×5.5-CL440	0.08	614	828.2	Y	749.8	1.10
108×79×5.5-CL440#	0.08	614	812.1	Y	737.5	1.10
108×79×5.5-CL850	0.26	1024	687.1	F	744.1	0.92
108×79×5.5-CL1200	0.29	1374	628.6	F	733.9	0.86
108×79×5.5-CL1500	0.48	1674	596.0	F	741.6	0.80
108×79×5.5-CL1500#	0.12	1674	582.3	F	752.9	0.77
125×85×6.5-CL200	0.56	374	1174.6	Y	983.4	1.19
125×85×6.5-CL440	0.01	614	1103.2	Y	984.7	1.12

^: Considering the cold-forming enhancement.

Y = Cross-section yielding failure; F = Flexural buckling failure.

Table 3. SOHS pin-ended column test results

Specimen	P_{Exp}/P_{FE}			P_{Exp}/P_{FE}			
	Corner Extension			Local imperfection+Global imperfection			
	t	$2t$	$2.5t$	$t/16+L/1500$	$t/16+L/3500$	$t/50+ L/1500$	$t/50+ L/3500$
93×62×5.5-CL200	1.03	1.03	1.03	1.04	1.04	1.04	**1.03**
93×62×5.5-CL440	1.02	1.02	1.02	1.03	1.02	1.03	**1.02**
93×62×5.5-CL850	0.99	0.99	0.99	1.03	1.03	1.03	**1.03**
93×62×5.5-CL1200	0.86	0.86	0.87	0.90	0.90	0.90	**0.90**
93×62×5.5-CL1500	0.87	0.88	0.88	0.93	0.93	0.93	**0.93**
107×68×6.5-CL200	1.09	1.09	1.09	1.11	1.10	1.10	**1.10**
107×68×6.5-CL440	1.03	1.03	1.03	1.03	1.03	1.03	**1.03**
107×68×6.5-CL850	0.97	0.98	0.98	1.01	1.01	1.01	**1.01**
107×68×6.5-CL1200	0.95	0.96	0.97	1.00	1.00	1.00	**1.00**
107×68×6.5-CL1500	0.93	0.94	0.95	1.03	1.03	1.03	**1.03**
108×79×5.5-CL200	1.04	1.04	1.04	1.05	1.05	1.04	**1.04**
108×79×5.5-CL440	1.02	1.02	1.02	1.03	1.03	1.03	**1.03**
108×79×5.5-CL440#	1.02	1.02	1.02	1.02	1.02	1.02	**1.02**
108×79×5.5-CL850	0.96	0.96	0.96	0.99	0.99	0.99	**0.99**
108×79×5.5-CL1200	1.04	1.04	1.04	1.07	1.07	1.07	**1.07**
108×79×5.5-CL1500	1.09	1.09	1.09	1.12	1.12	1.12	**1.12**
108×79×5.5-CL1500#	1.08	1.08	1.08	1.08	1.08	1.08	**1.08**
125×85×6.5-CL200	1.04	1.04	1.03	1.06	1.06	1.04	**1.04**
125×85×6.5-CL440	1.09	1.09	1.08	1.09	1.09	1.09	**1.09**
Mean	1.01	1.01	1.01	1.03	1.03	1.03	**1.03**
COV	0.069	0.065	0.063	0.052	0.052	0.051	**0.051**

Table 4. Summary of sensitivity study

Specimen	P_{FE} (kN)	Specimen	P_{FE} (kN)
450×360×20-CL1200	14231.2	350×200×2.5-CL1200	460.5
450×360×20-CL1900	12975.9	350×200×2.5-CL1900	451.1
450×360×20-CL2600	12507.4	350×200×2.5-CL2600	441.0
450×360×20-CL3300	12090.6	350×200×2.5-CL3300	430.1
450×360×20-CL4000	11694.8	350×200×2.5-CL4000	418.0
450×360×10-CL1200	6715.9	300×240×6-CL1200	2468.5
450×360×10-CL1900	6626.3	300×240×6-CL1900	2467.7
450×360×10-CL2600	6511.0	300×240×6-CL2600	2464.0
450×360×10-CL3300	6322.6	300×240×6-CL3300	2347.6
450×360×10-CL4000	6126.8	300×240×6-CL4000	2232.4
450×360×3-CL1200	738.5	245×140×4-CL1000	995.2
450×360×3-CL1900	728.2	245×140×4-CL1750	993.4
450×360×3-CL2600	717.8	245×140×4-CL2500	987.0
450×360×3-CL3300	704.1	245×140×4-CL3250	968.1
450×360×3-CL4000	686.8	245×140×4-CL4000	931.3
450×300×16-CL1200	10509.1	240×160×6-CL1000	1970.3
450×300×16-CL1900	9828.6	240×160×6-CL1750	1868.6
450×300×16-CL2600	9497.1	240×160×6-CL2500	1746.0
450×300×16-CL3300	9187.6	240×160×6-CL3250	1623.0
450×300×16-CL4000	8870.6	240×160×6-CL4000	1491.9
450×300×10-CL1200	6092.6	240×160×3-CL1000	580.5
450×300×10-CL1900	6072.2	240×160×3-CL1750	567.2
450×300×10-CL2600	6016.8	240×160×3-CL2500	555.2
450×300×10-CL3300	5886.0	240×160×3-CL3250	543.7
450×300×10-CL4000	5712.4	240×160×3-CL4000	533.5
450×300×3-CL1200	703.7	240×160×2-CL1000	288.6
450×300×3-CL1900	693.7	240×160×2-CL1750	278.3
450×300×3-CL2600	682.6	240×160×2-CL2500	266.7
450×300×3-CL3300	667.5	240×160×2-CL3250	254.5
450×300×3-CL4000	654.3	240×160×2-CL4000	241.2
450×225×20-CL1200	11808.1	200×160×16-CL1000	4188.7
450×225×20-CL1900	10968.2	200×160×16-CL1750	3812.3
450×225×20-CL2600	10587.9	200×160×16-CL2500	3459.1
450×225×20-CL3300	10218.4	200×160×16-CL3250	3168.5
450×225×20-CL4000	9840.4	200×160×16-CL4000	2865.4
450×225×4-CL1200	1094.9	200×160×3-CL1000	597.8
450×225×4-CL1900	1083.8	200×160×3-CL1750	586.1
450×225×4-CL2600	1075.2	200×160×3-CL2500	571.8

450×225×4-CL3300	1055.6	200×160×3-CL3250	554.4
450×225×4-CL4000	1043.8	200×160×3-CL4000	533.0
450×225×3-CL1200	665.4	200×160×2-CL1000	283.2
450×225×3-CL1900	657.0	200×160×2-CL1750	272.2
450×225×3-CL2600	648.2	200×160×2-CL2500	258.1
450×225×3-CL3300	635.5	200×160×2-CL3250	244.5
450×225×3-CL4000	625.9	200×160×2-CL4000	231.3
450×200×16-CL1200	8977.6	180×120×10-CL1000	2263.1
450×200×16-CL1900	8629.0	180×120×10-CL1750	2044.5
450×200×16-CL2600	8356.4	180×120×10-CL2500	1833.6
450×200×16-CL3300	8073.3	180×120×10-CL3250	1659.9
450×200×16-CL4000	7768.5	180×120×10-CL4000	1460.2
450×200×10-CL1200	5209.7	180×120×3.5-CL1000	787.7
450×200×10-CL1900	5086.0	180×120×3.5-CL1750	777.0
450×200×10-CL2600	5050.3	180×120×3.5-CL2500	724.6
450×200×10-CL3300	5001.8	180×120×3.5-CL3250	631.4
450×200×10-CL4000	4915.4	180×120×3.5-CL4000	545.1
450×200×2.5-CL1200	473.7	180×120×2-CL1000	261.0
450×200×2.5-CL1900	454.5	180×120×2-CL1750	250.8
450×200×2.5-CL2600	462.4	180×120×2-CL2500	239.5
450×200×2.5-CL3300	453.9	180×120×2-CL3250	230.2
450×200×2.5-CL4000	447.6	180×120×2-CL4000	222.1
450×180×16-CL1200	8707.8	180×80×8-CL1000	1625.5
450×180×16-CL1900	8387.4	180×80×8-CL1750	1461.8
450×180×16-CL2600	8122.4	180×80×8-CL2500	1288.0
450×180×16-CL3300	7844.0	180×80×8-CL3250	1147.5
450×180×16-CL4000	7539.7	180×80×8-CL4000	1001.4
450×180×10-CL1200	4937.8	180×80×2-CL1000	256.8
450×180×10-CL1900	4852.8	180×80×2-CL1750	250.1
450×180×10-CL2600	4836.1	180×80×2-CL2500	238.9
450×180×10-CL3300	4791.8	180×80×2-CL3250	224.9
450×180×10-CL4000	4727.2	180×80×2-CL4000	210.5
450×180×5.5-CL1200	1837.3	150×75×8-CL1000	1333.0
450×180×5.5-CL1900	1835.3	150×75×8-CL1750	1157.8
450×180×5.5-CL2600	1831.5	150×75×8-CL2500	1007.5
450×180×5.5-CL3300	1831.6	150×75×8-CL3250	863.2
450×180×5.5-CL4000	1830.8	150×75×8-CL4000	710.0
450×180×4-CL1200	1091.1	150×75×2.5-CL1000	363.8
450×180×4-CL1900	1094.5	150×75×2.5-CL1750	360.5
450×180×4-CL2600	1093.5	150×75×2.5-CL2500	337.4

450×180×4-CL3300	1073.7	150×75×2.5-CL3250	291.8
450×180×4-CL4000	1065.9	150×75×2.5-CL4000	253.7
420×240×20-CL1200	11381.0	150×60×6-CL1000	968.2
420×240×20-CL1900	10515.6	150×60×6-CL1750	840.9
420×240×20-CL2600	10138.1	150×60×6-CL2500	722.9
420×240×20-CL3300	9749.1	150×60×6-CL3250	616.4
420×240×20-CL4000	9357.6	150×60×6-CL4000	505.8
420×240×8-CL1200	3842.2	150×60×2-CL1000	231.4
420×240×8-CL1900	3837.5	150×60×2-CL1750	226.6
420×240×8-CL2600	3872.1	150×60×2-CL2500	210.1
420×240×8-CL3300	3874.2	150×60×2-CL3250	193.2
420×240×8-CL4000	3853.3	150×60×2-CL4000	176.0
420×240×2.5-CL1200	488.6	140×80×8-CL1000	1270.4
420×240×2.5-CL1900	477.7	140×80×8-CL1750	1094.5
420×240×2.5-CL2600	470.6	140×80×8-CL2500	952.1
420×240×2.5-CL3300	460.0	140×80×8-CL3250	799.4
420×240×2.5-CL4000	450.8	140×80×8-CL4000	642.1
350×200×8-CL1200	3532.0	140×80×2-CL1000	247.9
350×200×8-CL1900	3505.8	140×80×2-CL1750	241.0
350×200×8-CL2600	3439.1	140×80×2-CL2500	230.2
350×200×8-CL3300	3312.2	140×80×2-CL3250	212.0
350×200×8-CL4000	3170.8	140×80×2-CL4000	182.3

Table 5. Parametric study on cold-formed steel SOHS pin-ended columns

Number of specimen			$\frac{P_u}{P_{DSM}}$	$\frac{P_u}{P_{DSM}{}^*}$
Test:19	FE:200			
Non-slender section: 84 ($\lambda_l \leq 0.702$)	Short: 20 ($\lambda_c \leq 0.25$)	Mean	1.17	1.06
		COV	0.093	0.090
		ϕ	0.85	0.85
		β	3.22	2.84
	Medium and long: 64 ($\lambda_c > 0.25$)	Mean	1.02	1.00
		COV	0.047	0.039
		ϕ	0.85	0.85
		β	2.86	2.79
Slender section: 135 ($\lambda_l > 0.702$)		Mean	0.98	1.04
		COV	0.104	0.071
		ϕ	0.85	0.85
		β	2.53	2.89
ALL: 219		Mean	1.01	1.03
		COV	0.104	0.069
		ϕ	0.85	0.85
		β	2.64	2.85

*: Modified design method

Table 6. Comparison of SOHS pin-ended column test and FE results with predicted strengths